



## CYCLIC PERFORMANCE OF LOADBEARING MASONRY WALLS WITH REACTIVE BOUNDARY CONDITIONS

C. Pettit<sup>(1)</sup>, A. Ba Rahim<sup>(2)</sup>, O. Guzman-Sanchez<sup>(3)</sup>, C. Cruz-Noguez<sup>(4)</sup>

<sup>(1)</sup> Ph.D. Student, University of Alberta, [cpettit@ualberta.ca](mailto:cpettit@ualberta.ca)

<sup>(2)</sup> Ph.D. Student, University of Alberta, [abarahim@ualberta.ca](mailto:abarahim@ualberta.ca)

<sup>(3)</sup> Ph.D. Student, University of Alberta, [guzmansa@ualberta.ca](mailto:guzmansa@ualberta.ca)

<sup>(4)</sup> Associate Professor, University of Alberta, [cruznogu@ualberta.ca](mailto:cruznogu@ualberta.ca)

### **Abstract**

Loadbearing masonry walls are commonly seen across North America in low-rise commercial and industrial settings as they provide a competitive structural solution to resist a combination of out-of-plane (OOP) and gravity loads. During the construction of these walls, concrete masonry units (CMU) are placed upon concrete footing foundations in which the extruding steel dowels of the footing are embedded into the grouted cells of the wall. This embedment creates a connection between the masonry wall and concrete footing, resulting in a rotational stiffness at the base of the wall. North American design standards, however, neglect this base stiffness as concerns about the possible degradation of the connection under cyclic loads have arisen. An experimental program designed to assess the cyclic performance of moderately slender reinforced masonry walls with a base stiffness is proposed in this study. Magnitudes of rotational base stiffness provided from typical foundations were determined by modeling the foundation's geometry and soil interaction in the finite-element (FE) program OpenSEES. Of the variety of foundations modeled, those considered to be the most typical in the construction industry were later simulated during the experimental testing. The experimental program involved the testing of 4 identical partially grouted CMU masonry walls. Each specimen was tested under with a constant axial load and a cyclic lateral load. The rotational stiffness provided at the base of each wall was varied between specimens and ranged from 0 kNm/radian (pinned) to 9,500 kNm/radian. The response of the specimens with a rotational base stiffness was then compared to the pinned specimen to determine the influence of rotational base stiffness on loadbearing capacity, ductility, and flexural rigidity. The insights gained regarding the influence of a rotational base stiffness on loadbearing masonry walls are presented and discussed.

*Keywords: Masonry, Cyclic, Out-of-Plane, Base Stiffness, Gravity and Lateral Loads*



## 1. Introduction

Slender, loadbearing masonry walls are an efficient system to resist out-of-plane (OOP) and gravity loads. Although slender loadbearing masonry walls are a common structural solution for low- to mid-rise construction, the behavior of these walls is still relatively uncertain. The Canadian standard for masonry design [1] calls for stringent design procedures which recent research [2,3,4,5] has found to be overly conservative, and not being reflective of the true performance of these walls, measured during experiments or calculated with sophisticated finite-element models.

One of the most significant design provisions in the current code is the assumption of a pinned base for walls with slenderness ratios ( $kh/t$ ) greater than 30. This provision neglects the effect of the rotational support stiffness provided at the base of the wall, which has been shown to both increase the loadbearing capacity and limit OOP deflections of slender loadbearing walls [3]. It could be argued that the pinned base assumption might have validity under realistic loading conditions: these would impose cyclic force demands at the base, causing degradation of the masonry and the steel reinforcement at the connection – eventually, turning it into a hinge.

It is difficult to assess the validity of this assumption as most of the available studies for over 40 years consisting of walls tested with pinned-pinned boundary conditions. Mohsin [3] was one of the first who investigated the role of non-zero rotational base stiffness on loadbearing masonry walls. The study comprised of an experimental program in which 8 slender masonry wall specimens with varying base stiffness were tested under an eccentric axial load. Results from the study showed the presence of a base rotational stiffness significantly reduced second-order effects by limiting the OOP deflections and increased the loadbearing capacity of the walls as much as 87.5%. Comparisons of the effective flexural rigidity obtained during the experimental program to those calculated using the Canadian standard [1] indicated vast conservatism in the code as experimental values were up to 5.1 times greater than those calculated using the standard. However, the study is limited as the presence of a lateral load (often the governing load in slender masonry wall design) was absent along with any type of cyclic loading.

To further test the validity of a pinned base assumption, this study aims to provide experimental insight on the influence that a rotational base stiffness has on the key structural parameters, such as strength, stiffness, and energy dissipation, of loadbearing masonry walls under cyclic loading. It is noted that the wall specimens in the study were limited to a slenderness ratio ( $kh/t$ ) of 12 which is defined by CSA S304 as moderately slender. For these walls, CSA S304 permits the inclusion of the base stiffness in the determination of the flexural rigidity of the wall. The moderately slender walls used in this study ( $kh/t < 30$ ) constitute a first step towards investigating slender walls ( $kh/t > 30$ ), which will be addressed in future studies. This is because there are several novel aspects in this study, the implications of which could impact or influence the design of the next experimental phase. For instance, to the knowledge of the authors, this is the first study that incorporates the effects of a cyclic lateral load. The degradation of the connection at the base and related rotational mechanics are factors that will be important to consider when taller walls are tested, as an unintended (brittle) failure at the connection could hinder the experiments and present serious safety concerns.

## 2. Numerical Estimation of Rotational Support Stiffness

Prior to beginning the experimental program, a numerical simulation using the open-source finite element (FE) program OpenSEES was conducted to determine the rotational support stiffness provided by typical shallow strip footing foundations. Strip footings were selected in this study as they are commonly used for masonry walls due to their continuous spans and ability to spread the gravity loads within the wall across an area of soil. Soil piles were excluded as loadbearing masonry walls are often lightly loaded axially and do not require the additional bearing capacity. The magnitude of rotational restraint these foundations provide at the base of the wall is a function of the soil properties and foundation geometry. An FE model capable of analyzing the behavior of strip footing foundations was developed and was used to determine the rotational support stiffness



values to be used in the experimental program. The simulation of the rotational support stiffness in the experimental setup is discussed in a later section.

## 2.1 Finite Element Model for Strip Footing Foundations

Foundations were modeled as a 2D series of nodes connected by nonlinear beam-column elements (Fig. 1a). The constitutive material behavior of the elements was defined using the pre-defined Concrete02 material model. The model is a Kent and Park [6] concrete model with degrading linear unloading/reloading stiffness as per the work of Karsan and Jirsa [7]. A concrete compressive strength ( $f'_c$ ) of 30 MPa was specified for all elements in the model. A linear response for the soil was assumed, and the soil-foundation interaction was captured by defining elastic springs along the bottom edge of the foundation. The stiffness of each spring was calculated to correspond to the modulus of subgrade reaction of the soil multiplied by the base area of the footing.

As the objective was to calculate the rotational stiffness of the foundation, an applied moment was specified at the top of the foundation for the analysis. This moment was increased throughout the analysis until the rotation at the top of the foundation (Fig. 1b) reached a value of 1 radian. The corresponding moment to cause this rotation was taken as the rotational support stiffness (units of kNm/radian). The soil was assumed elastic and the rotational support stiffness of the foundation was assumed to be a function of the foundation's geometry and the modulus of subgrade solely for the underlying soil (the effect of side soil is neglected). It is assumed that the top of the footing does not move laterally under the applied moment.

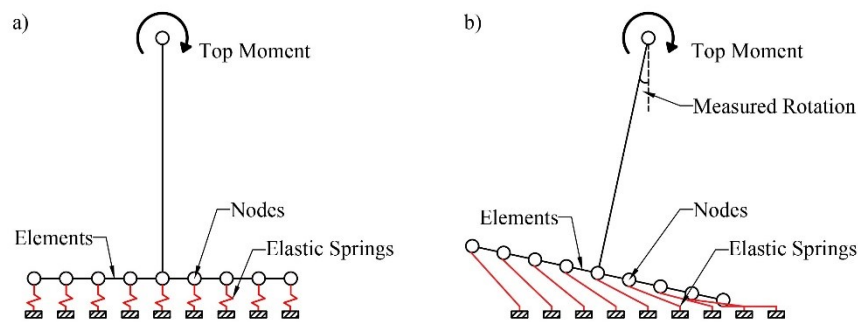


Fig. 1 – Finite Element Model a) Prior to Analysis b) During Analysis

## 2.2 Support Stiffness Assessment

Two wall types were considered in the calculation of rotation stiffness: slender, single-story masonry walls and multi-story, non-slender masonry walls. Slender, single-story masonry walls are typically subjected to lighter gravity loads (often just a roof load) than their multi-story counterparts but are much more susceptible to OOP bending due to their longer unsupported spans. The foundation design of slender walls is often governed by overturning moment, which results in a smaller foundation length than that of a non-slender wall, whose design is often governed by bearing capacity due to the large gravity loads present in the wall (a large foundation area is required to adequately distribute the loads).

Analyzing the foundations of slender masonry walls, the rotational stiffness provided ranges from 1,500 kNm/rad to 3,500 kNm/rad depending on the soil type. Foundations of non-slender multi-story masonry walls provide much larger rotational stiffnesses, ranging from 9,000 kNm/rad to 12,000 kNm/rad. Based on the results presented above, and experimental constraints (such as the practical length of the foundation beam used in the experimental test) three values of rotational stiffness were chosen for this investigation: 2,300 kNm/rad, 5,000 kNm/rad, and 9,500 kNm/rad. It is assumed that these cover a practical range of foundation rotational stiffnesses found in practice.



### 3. Experimental Program

#### 3.1 Test Specimens

Four wall specimens were constructed with standard 20-cm hollow concrete masonry units with a specified compressive strength of 15 MPa. Each specimen measured 12 courses (2.4 m) in height and 3 courses (1.2 m) wide. Specimens were constructed in running bond pattern by certified masons. All specimens were constructed on 1 in (25.4 mm) thick steel plates to accommodate the handling and transportation of the walls before and after testing.

Reinforcement detailing was designed to reflect typical masonry wall block design practices. Vertical reinforcement consisted of two 15M steel reinforcing bars located in the second cell from each end of the specimen (600 mm on center). Each bar was welded to the steel plate. Bond beams and bed joint reinforcement were used for horizontal reinforcement. Standard ladder joint reinforcement was placed every second course, while bond beams consisting of a single 15M steel reinforcing bar were located at the 1st, 6th, and 12th courses. All cells containing reinforcing steel were grouted with standard course grout. Reinforcing details are shown in Fig. 2.

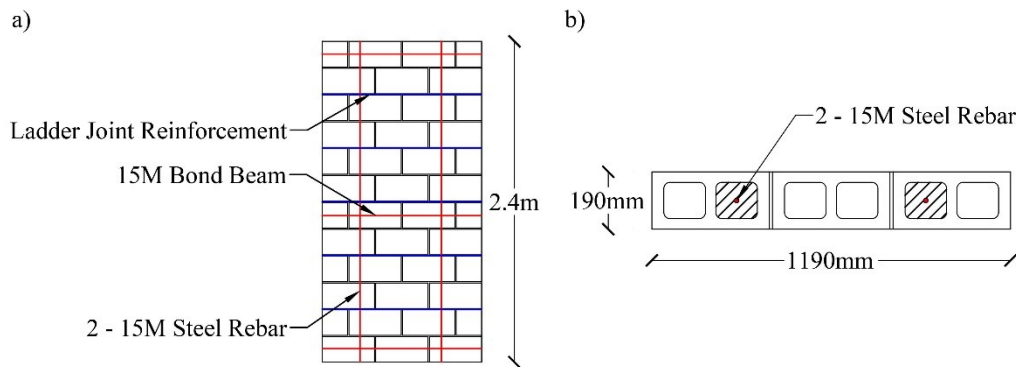


Fig. 2 – Specimen Reinforcing Details a) Elevation View b) Cross-Sectional View

#### 3.2 Material Properties

##### 3.2.1 Masonry

Masonry material properties were determined through testing 4" (101.6 mm) grout cylinders, 2" (50.8 mm) mortar cube and five-course prism tests (both grouted and ungrouted). Both the 4" (101.6 mm) grout cylinders and 2" (50.8 mm) mortar cube molds were filled with grout and mortar used during the construction of the wall specimens. Each was cured for a period of 28 days before being concentrically crushed. Crushing of the grout cylinders and mortar cubes revealed a peak compressive strength of 35.9 MPa and 13.8 MPa for the grout and mortar respectively. The strength of the masonry assemblage was determined through prism tests. A total of five ungrouted and grouted five-course prisms were constructed using the same materials as the masonry walls. Prisms were left to cure alongside the walls for a period of 28 days before being concentrically crushed with an MTS 6000 hydraulic ram. Testing revealed the compressive strength for the grouted and ungrouted prisms to be 16.8 MPa and 23.6 MPa respectively.

##### 3.2.2 Reinforcing Steel

All test specimens were constructed using grade 400 15M steel rebar from the same batch. Three standard tensile tests were conducted to determine the material properties of the rebar. Results from the tests indicated an average yield strength ( $f_y$ ) of 533 MPa and a modulus of elasticity ( $E_s$ ) of 198,817 MPa.

Based on the geometry of the wall and material properties of the masonry assemblage and reinforcing steel, the moment capacity of the wall specimens was calculated using the Canadian standard as 41.2 kNm.



### 3.3 Experimental Setup

The experimental setup used in this program consisted of three major parts: a lateral bracing system, a system for gravity and lateral load application, and the simulation of the rotational stiffness at the base of the wall specimens. Fig. 3 presents the complete experimental setup.

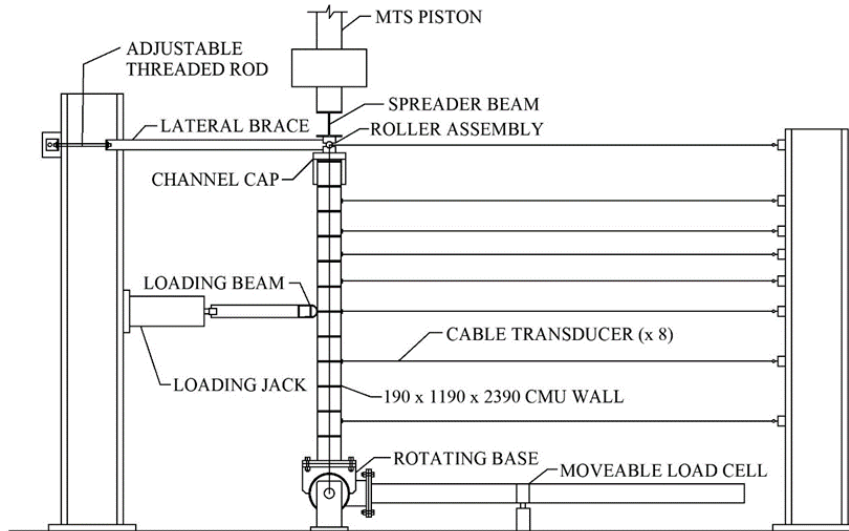


Fig. 3 – Experimental Setup

#### 3.3.1 Lateral Bracing System

The testing configuration was designed to simulate simple boundary conditions (i.e., a pinned bottom at the bottom of the wall with a lateral roller at the top). The bottom fixture (Fig. 4a) consists of a rotating steel cylinder to which the base plate of each wall was bolted to using a total of 10 (5 on each side of the wall) 1-in (25.4-mm) structural bolts. The cylinder itself is hinged between two steel plates that were secured to the strong floor of the lab with 1-in (25.4-mm) floor rods. This system allows for the base of the wall to rotate OOP freely while restricting any horizontal and vertical movement. The top fixture (Fig. 4b) utilizes a steel channel cap firmly secured to the top of the masonry wall. Two steel channels then have one end bolted to the top channel cap and the other the support column. To ensure no lateral displacement during testing, the channels connected to the channel cap featured an adjustable threaded rod. By tightening the bolts along the threaded rod, the wall can be readjusted into place during testing if lateral displacement at the top of the wall occurs.



Fig. 4 – a) Bottom Fixture b) Top Fixture

#### 3.3.2 Gravity and Lateral Load Application

The vertical load was applied to the top of the wall using an MTS 6000 hydraulic ram. To transfer the load from the MTS to the top of the wall, a steel loading beam was connected to the MTS crosshead (Fig. 5a).



Contact between the loading beam and channel cap was made through two pins on both ends of the loading beam. These pins allowed for the load to be transferred without restricting any rotation experienced by the top of the wall during testing.

The lateral load was applied to the wall in a three-point bending configuration. A loading jack with a capacity of 539 kN transferred the load through a steel spreader beam constructed of hollow structural steel (HSS) sections (Fig. 5b) to the wall. A Teflon strip was placed at the point of contact between the spreader beam and masonry wall to ensure a uniform distribution of load along the wall. The spreader beam was leveled before each test.



Fig. 5 – a) Gravity Load Application b) Lateral Load Application

### 3.3.3 Simulation of Base Rotational Stiffness

The rotational support stiffness at the base of the wall specimens was simulated by rigidly connecting a steel HSS beam to the bottom fixture of the test setup and simply supporting the other end on the laboratory floor (Fig. 6). This allows for the rotational support stiffness at the base of the wall to be approximately proportionate to the flexural stiffness of the steel section. In this study, an HSS 152 x 152 x 6.4-mm steel beam was selected. To achieve the desired values of support stiffness listed in section 2.2, the unsupported span of the beam was varied, with shorter and longer spans providing larger and smaller values of rotational support stiffness respectively. Details of the spans selected, and their respective rotational stiffness can be found in Table 1.



Fig. 6 – Simulation of the Base Rotational Stiffness

Table 1 – Simulated Base Rotational Stiffness

Specimen	Rotational Stiffness (kNm/rad)	HSS Section (mm)	HSS Section Span (m)
1	0	-	-
2	2,300	HSS 152 x 152 x 6.4	3.5
3	5,000	HSS 152 x 152 x 6.4	1.5
4	9,500	HSS 152 x 152 x 6.4	0.75



### 3.4 Instrumentation

Instrumentation consisted of strain gauges, load cells, inclinometers, and linear variable differential transformers (LVDTs), all connected electronically through 31 channels. Each vertical reinforcing bar contained 4 strain gauges: one located at the midpoint, two located 16 in (406 mm) above and below the midpoint, and one located 5 in (127 mm) above the base of the reinforcing bar. Four more strain gauges were also added to the outer compression face of the masonry blocks. Inclinometers were used to determine the rotation at the top and bottom supports for all tests. The lateral deflection was measured through 8 LVDTs placed over the height of the wall. More LVDTs were placed on the upper half of the wall to capture a possible rise in the location of maximum deflection. Load cells connected to the MTS and loading jack measured both the vertical and lateral loads during testing. An additional load cell was placed under the simply supported end of the HSS section used to simulate the rotational stiffness at the base of the wall.

### 3.5 Testing Procedure

The walls were tested in two steps. First, a vertical load was applied to the top of the specimens in load control using the MTS 6000 and held. All test specimens were loaded with an axial load of 250 kN (approximately 10% of the compressive capacity of the specimen; a value commonly used in practice). Then, a hydraulic jack was used to apply a cyclic lateral load to the midpoint of the wall in cycles until failure occurred. A loading rate of 2 mm/min was used for cycles 1 to 4 (made in 5-mm increments) and was then increased to 4 mm/min for the remainder of the test cycles (made in 10-mm increments). The loading protocol of the cycles is shown in Fig. 7.

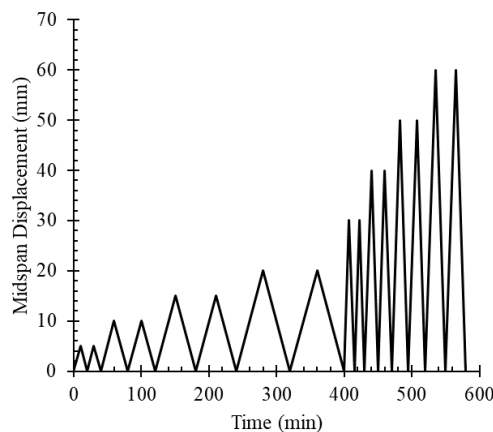


Fig. 7 – Cyclic Loading Protocol

### 3.6 Results and Observations

Results and observations noted during the testing of each wall are discussed below. All displacements and forces were obtained through LVDTs and load cells respectively. Rotations at the top and bottom of the wall were obtained with the clinometers. The lateral load-midspan displacement and lateral load-base rotation are presented in Fig. 8 and Fig. 9 respectively.

Specimen 1 was tested with zero rotational stiffness and acted as the reference wall in the experimental program. The specimen was able to complete all 8 cycles before failure occurred. The first sign of failure occurred during the 20-mm cycle when the separation between the masonry units and mortar joints near the midspan of the specimen was observed. The peak lateral load for the specimen was 52.2 kN with a corresponding midspan deflection of 29.5 mm. Failure occurred during the last cycle with the crushing of the masonry at the midspan (Fig. 10a). The midspan deflection at failure was 69.1 mm with a corresponding lateral load of 40.0 kN.

Specimen 2 was tested with a rotational stiffness of 2,300 kNm/rad at the base of the wall. The specimen was not able to complete all 8 cycles before failure occurred. The first sign of failure occurred during the 15-



mm cycle when the separation between the masonry units and mortar joints near the midspan of the specimen was observed. The peak lateral load for the specimen was 87.4 kN with a corresponding midspan deflection of 38.0 mm. Failure occurred during the first 60-mm cycle, with the simultaneous crushing of the masonry along the bottom half of the wall (Fig. 10b). The midspan deflection at failure was 50.6 mm with a corresponding lateral load of 76.7 kN.

Specimen 3 was tested with a rotational stiffness of 5,000 kNm/rad at the base of the wall. The specimen was not able to complete all 8 cycles before failure occurred. The first sign of failure occurred during the 10-mm cycle when the separation between the masonry units and mortar joints near the midspan of the specimen was observed. The peak lateral load for the specimen was 101 kN with a corresponding midspan deflection of 37.0 mm. Failure occurred during the first 50-mm cycle, with the crushing of the masonry at the midspan (Fig. 10c). The midspan deflection at failure was 40.9 mm with a corresponding lateral load of 94.0 kN.

Specimen 4 was tested with a rotational stiffness of 9,500 kNm/rad at the base of the wall. The specimen was not able to complete all 8 cycles before failure occurred. The first sign of failure occurred during the 10-mm cycle when the separation between the masonry units and mortar joints near the midspan of the specimen was observed. The peak lateral load for the specimen was 95.9 kN with a corresponding midspan deflection of 38.8 mm. Failure occurred during the first 50 mm cycle, with the crushing of the masonry at the midspan (Fig. 10d). The midspan deflection at failure was 43.2 mm with a corresponding lateral load of 90.7 kN.

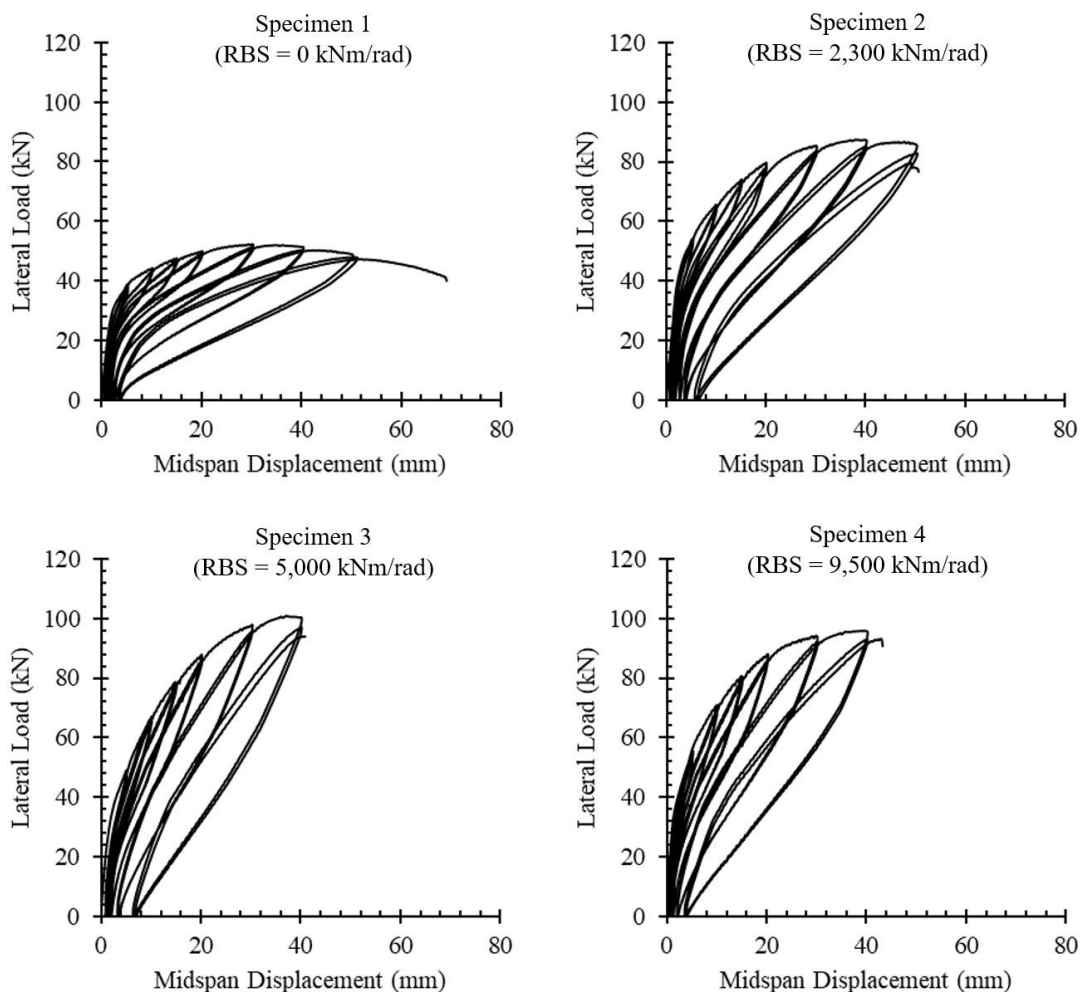


Fig. 8 – Lateral Load-Midspan Displacement Response

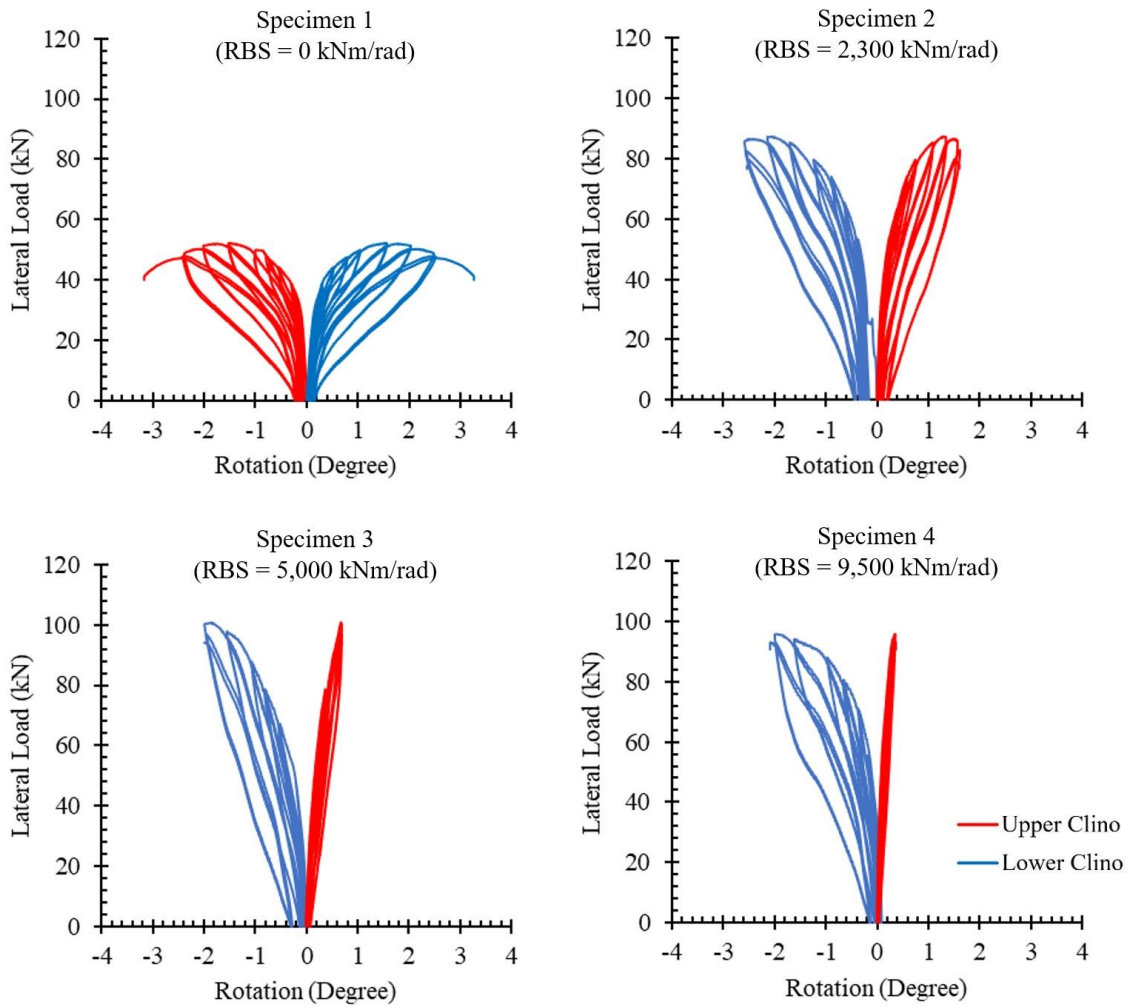


Fig. 9 – Lateral Load-Base Rotation Response

Specimen 1                      Specimen 2                      Specimen 3                      Specimen 4

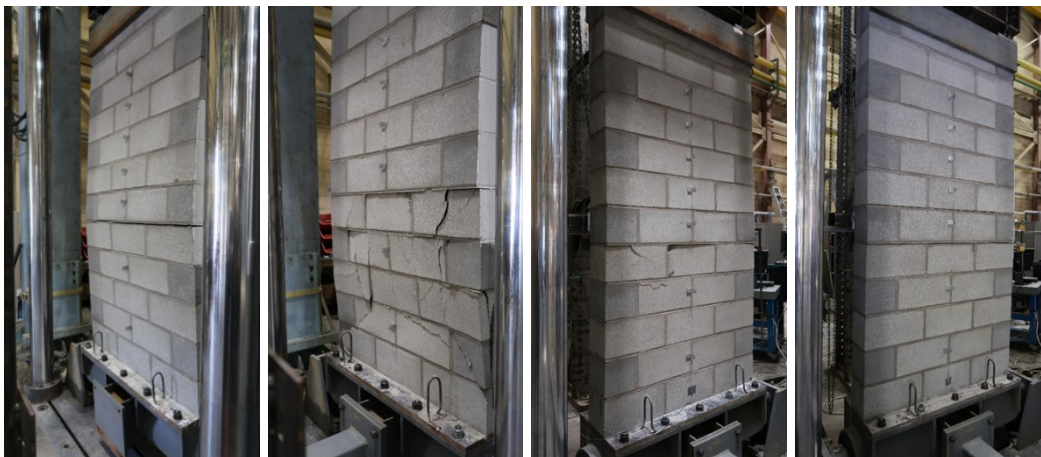


Fig. 10 – Specimens after Failure Occurs



## 4. Discussion

### 4.1 Loadbearing Capacity, Midspan Deflection, and Base Rotation

Plotting the backbone curves of the 4 test specimens (Fig. 11a) shows that, in general, as the level of rotational base stiffness (RBS) is increased, the lateral load-carrying capacity of the wall increase, while the ultimate midspan deflections decrease. This is because the presence of rotational support stiffness at the base of the wall creates a negative moment sub-profile over the height of the wall proportional to the amount of base support stiffness. This negative moment sub-profile redistributes the total moment profile over the height of the wall resulting in smaller bending moments at the midspan region for walls with a larger base support stiffness, compared to walls with a smaller base support stiffness at the same values of lateral load.

The lateral load-carrying capacity increase is not linear with the increase in base rotational support stiffness. As the rotational base stiffness is increased, the increase in lateral load capacity begins to plateau. When increasing the base support stiffness from 0 kNm/rad to 2,300 kNm/rad, the lateral load-carrying capacity of the specimens increased from 52.5 kN to 87.4 kN (a relative increase of 66%), while increasing the base stiffness from 2,300 kNm/rad to 9,500 kNm/rad only increased the load-carrying capacity of the specimens from 87.4 kN to 95.9 kN (a relative increase of 10%). This is attributed to the base rotational support stiffness approaching the fixed-pinned boundary condition, which acts as an upper limit on the benefit received from base support stiffness. The relative increase of lateral load capacity with base rotational stiffness is presented in Table 2.

Fig. 11b shows the base rotation of the specimens as reported by the lower clinometer under applied levels of lateral load. As expected, specimens with higher base rotational support stiffness experienced a lower base rotation compared to those with lower stiffness. Comparing Specimen 1 (RBS = 0 kNm/rad) to Specimen 4 (RBS = 9,500 kNm/rad) at failure, Specimen 4 reported an 89% relative decrease in base rotation as compared to Specimen 1. An interesting phenomenon displayed in the figure is the behavior of the base rotation. As the level of base support stiffness was increased, the behavior of the base rotation transitioned from a nonlinear to a more linear behavior.

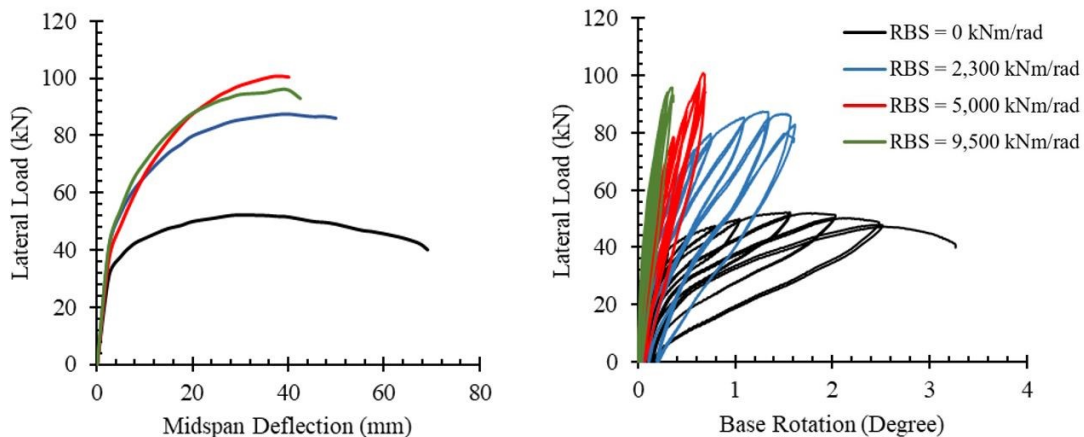


Fig. 11 – a) Backbone Lateral Load-Midspan Displacement Comparison b) Base Rotation Comparison

One anomaly in the experiment was the response of Specimen 3 (base rotational stiffness of 5,000 kNm/rad). The response of Specimen 3 was rather unexpected, as it demonstrated a higher bending moment capacity than the other specimens. In fact, the reported load-carrying capacity of the specimen was higher than that of Specimen 4, even though Specimen 4 featured a higher base rotational support stiffness. Upon further inspection, the reason for this was the misplacement of the reinforcing steel in Specimen 3. Forensic examination showed that the reinforcing steel in Specimen 3 had been placed approximately 2 cm closer to the tension face of the wall compared to other specimens, resulting in a relative increase in bending moment capacity of 10.4%. The reinforcing steel placement in the other 3 specimens was found to be adequate. If the



bars in specimen 3 had been placed in the middle of the cell, the predicted increase in lateral capacity, relative to Specimen 1, would have been 83.7%, in line with the results in Table 2.

Table 2 – Relative Increase in Lateral Load Capacity

Specimen	Increase in Base Stiffness (kNm/rad)	Increase in Lateral Load Capacity to Wall 1 (pinned)
2	0 to 2,300	66.5%
3	0 to 5,000	92.4%
4	0 to 9,500	82.7%

#### 4.2 Deflection and Total Moment Profiles at Failure

Fig. 12a and 12b depict the deflection and total moment profile over the height of the wall specimens at failure respectively. It should be noted that the bottom point of rotation rested in the steel fixture and not the base of the wall which is why non-zero deflections are recorded at the base of the wall (Fig. 12a). Referring to Fig. 12b, it is seen that the magnitude of the base moment increased with increased support stiffness. Additionally, the presence of a base stiffness created an inflection point indicating the wall acts in double curvature (as seen in Fig. 12a). As the base stiffness increased, the point of inflection moved up the height of the wall. This is expected, as the presence of a larger base rotational stiffness creates a larger base moment, resulting in a larger negative moment profile.

At failure, the largest moment magnitude was a positive moment located at the midspan for Specimens 1, 3 and 4. The largest moment magnitude for Specimen 2, however, was a negative moment located at the base of the wall. This was due to the relatively large base rotations (as compared to the other specimens with a rotational base stiffness) sustained by Specimen 2 during testing. After peak load, the lateral load placed on the wall begins to decrease resulting in a decrease in the first-order moment profile. However, the wall deflection and rotation at the base of the specimen continue to increase. As a result, the second-order and support moment profiles continue to grow in magnitude. In fact, the tests showed that in all cases where the specimen featured a base stiffness, the support moment profile increased at a higher rate than the second-order profile (the first-order moment is decreasing). This caused the total moment at the midspan of the walls to decrease during the post-peak response.

Comparing the maximum moments sustained by each specimen to the predicted moment capacity (41.2 kNm), all specimens exceeded the predicted moment capacity. As all specimens were able to exceed the predicted moment capacity under a cyclic load, this indicates that the degradation of the base of the wall due to the rotational base stiffness does not have a significant reduction in the ultimate moment capacity of the wall.

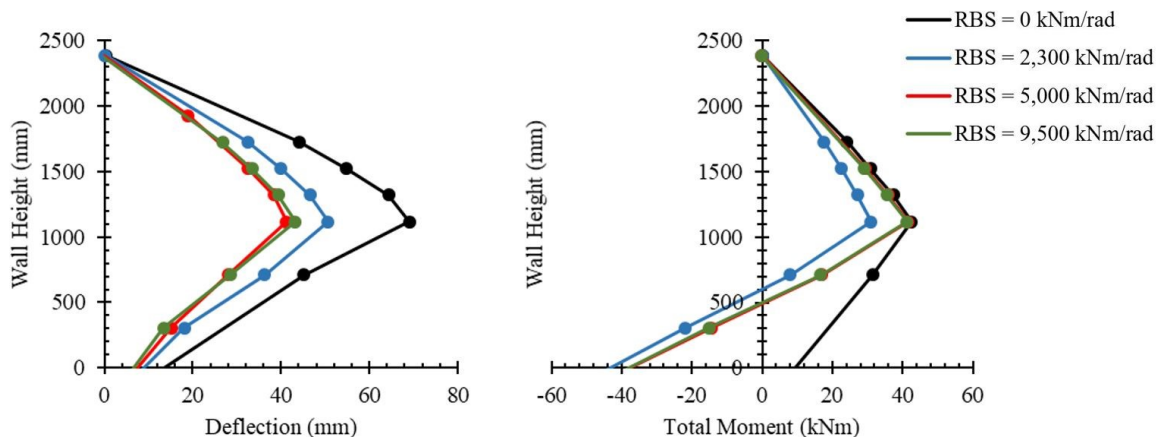


Fig. 12 – a) Deflection Profile at Failure b) Total Moment Profile at Failure



## 5. Conclusions

To determine the effects of a rotational base stiffness on the loadbearing capacity and degradation of flexural masonry walls, an experimental program dealing with four wall specimens was introduced. All four wall specimens were identical in geometry and material properties with the only variation between specimens being the level of rotational stiffness found at the base of the wall. Each wall was tested under a combination of axial and cyclic lateral loads. The axial load placed on all specimens was 250 kN (representing roughly 10% of the wall's axial capacity). Following the axial load, each load was laterally loaded cyclically in a three-point bending scheme. Initial cycles were conducted in increments of 5 mm of midspan deflection. Once 20 mm of midspan deflection was reached, the cycle increment was increased to 10 mm and continued until failure occurred. Every cycle was repeated twice. All wall specimens failed with the crushing of the masonry at the midspan, however, specimens that featured a rotational base stiffness exhibited additional damage along the lower half of the wall compared to the wall specimen without a rotational base stiffness. Test results indicate the presence of a rotational base stiffness results in an increase in lateral loadbearing capacity and a decrease in both base rotation and OOP deflections. No significant base degradation under the cyclic lateral load was observed during the test indicating that the assumption of a pinned base during masonry wall design is perhaps conservative. Although promising, more experimental tests dealing with slender loadbearing walls with a rotational base stiffness subject to cyclic lateral loads are required before any conclusions are drawn about the benefits of using a rotational base stiffness in loadbearing masonry wall design.

## 6. Acknowledgments

The authors would like to thank the lab technicians, Greg Miller and Cameron West, for all their help during the testing process as well as both Expocrete and Scorpio Masonry Inc. for their aid in funding both the materials and construction of the test specimens. Additional thanks are also required for the Canadian Masonry Design Centre (CMDC) for the valuable technical advice received.

## 7. References

- [1] Canadian Standards Association (2014). "Design of Masonry Structures." CSA S304-14. Rexdale, ON, Canada
- [2] Liu, Y., and Dawe, J. L. (2001). "Experimental determination of masonry beam-column behaviour." *Canadian Journal of Civil Engineering*, 28(5), 794–803.
- [3] Mohsin, E. (2005). "Support Stiffness Effect on Tall Load Bearing Masonry Walls." University of Alberta.
- [4] Liu, Y., and Hu, K. (2007). "Experimental study of reinforced masonry walls subjected to combined axial load and out-of-plane bending." *Canadian Journal of Civil Engineering*, 34(11), 1486–1494.
- [5] Isfeld, A. C., Müller, A. L., Hagel, M., and Shrive, N. G. (2019). "Analysis of safety of slender concrete masonry walls in relation to CSA S304-14." *Canadian Journal of Civil Engineering*, 46(5), 424–438.
- [6] Kent, D.C., and Park, R. (1971) "Flexural members with confined concrete", *Journal of the Structural Division*, ASCE, 97(7), pp. 1969-1990.
- [7] Karsan, I.D., and Jirsa, J.O. (1969), "Behavior of concrete under compressive loadings", *Journal of the Structural Division*, ASCE, 95(ST12), pp. 2543-2563.